Journal of Power Sources 196 (2011) 7372–7382

Contents lists available at ScienceDirect

Journal of Power Sources

journal homepage: www.elsevier.com/locate/jpowsour

Impact of substrate material and annealing conditions on the microstructure and chemistry of yttria-stabilized-zirconia thin films

Barbara Scherrer[a,*], Antonella Rossi[b,c], Julia Martynczuk[a], Marta D. Rossell[d], Anja Bieberle-Hütter[a], Jennifer L.M. Rupp[a], Rolf Erni[e], Ludwig J. Gauckler[a]

[a] ETH Zurich, Nonmetallic Inorganic Materials, HCI G536, Wolfgang-Pauli-Str. 10, 8093 Zurich, Switzerland
[b] ETH Zurich, Surface Science and Technology, Wolfgang-Pauli-Str. 10, CH-8093 Zurich, Switzerland
[c] Università degli Studi di Cagliari, Cittadella Universitaria Monserrato, I-09100 Cagliari, Italy
[d] ETH Zurich, Multifunctional Materials, Wolfgang-Pauli-Str. 10, CH-8093 Zurich, Switzerland
[e] Empa, Swiss Federal Laboratories for Materials Science and Technology, Electron Microscopy Center, Ueberlandstr. 129, CH-8600 Dübendorf, Switzerland

ARTICLE INFO

Article history:
Received 4 January 2011
Received in revised form 4 March 2011
Accepted 27 March 2011
Available online 5 April 2011

Keywords:
Micro-solid oxide fuel cell
MEMS
Silicon diffusion
Yttria-stabilized-zirconia
Thin film
Spray pyrolysis

ABSTRACT

Si-diffusion from Si-based substrates into yttria-stabilized-zirconia (YSZ) thin films and its impact on their microstructure and chemistry is investigated. YSZ thin films used in electrochemical applications based on micro-electrochemical systems (MEMS) are deposited via spray pyrolysis onto silicon-based and silicon-free substrates, i.e. Si_xN_y-coated Si wafer, SiO_2 single crystals and Al_2O_3, sapphire. The samples are annealed at 600 °C and 1000 °C for 20 h in air. Transmission electron microscopy (TEM) showed that the Si_xN_y-coated Si wafer is oxidized to SiO_z at the interface to the YSZ thin film at temperatures as low as 600 °C. On all YSZ thin films, silica is detected by X-ray photoelectron spectroscopy (XPS). A particular large Si concentration of up to 11 at% is detected at the surface of the YSZ thin films when deposited on silicon-based substrates after annealing at 1000 °C. Their grain boundary mobility is reduced 2.5 times due to the incorporation of SiO_2. YSZ films on Si-based substrates annealed at 600 °C show a grain size gradient from the interface to the surface of 3 nm to 10 nm. For these films, the silicon content is about 1.5 at% at the thin film's surface.

1. Introduction

The pure oxygen-ion conductivity qualifies yttria-stabilized-zirconia thin films (YSZ, $Zr_{0.85}Y_{0.15}O_{2-\delta}$) as a functional material in oxygen separation membranes, oxygen sensors and electrolytes in solid oxide fuel cells (SOFCs) [1]. Recently, YSZ was introduced as functional thin film in micro-electro-mechanical systems (MEMS) such as micro-SOFCs for power generation and replacement of batteries in portable electronics [2–16]. For this kind of devices, YSZ thin films are integrated on substrates which are mostly based on silicon, e.g. Si-wafer coated with insulating layers such as SiO_2 or Si_xN_y [11–14,16] or silicon-based Foturan® glass-ceramic wafer [6]. In contrast to traditional MEMS-based devices, micro-SOFCs are operated at rather high temperatures of 250–600 °C in order to ensure sufficient oxygen-ion conductance in YSZ. In view of application in micro-SOFCs, it is important to study the stability of the YSZ–Si interface as inter-diffusion or reactions are likely to occur and may affect the electrical performance of the micro-SOFC.

Literature reports the effect of silica on the microstructural and electrical properties of bulk YSZ. Silica is found as impurity in the raw powders for YSZ pellets, or can additionally be incorporated during annealing from Si-contaminations in the furnace. Silica is soluble in YSZ up to concentrations of 0.3 wt% [17]. Pure YSZ powders have normally around 0.003 wt% silica, less pure YSZ contains 0.03 wt% SiO_2 [18,19]. It has been shown that silica segregates during heat treatment to the grain boundaries and to the surface of a sintered pellet [20–24] with 800 °C being the lowest temperature at which silica was detected after 5 h heating [20].

Silica impurities play an important role in the microstructure evolvement during thermal treatment of YSZ pellets [17,18,20–24]. The segregation of Si into the grain boundary reduces their mobility and acts as impurity drag-force on grain growth [19]. As a result, grain growth kinetics show increased non-parabolic grain growth exponents [25] already at low silica concentration of 0.05 wt% in YSZ [18]. The impeded grain growth kinetics lowers the mean grain sizes, i.e. for 0.05 wt% silica up to 30% relative to impurity-free YSZ, if sintered at 1350 °C for 5 h [18]. Also other impurities segregate to the surface and grain boundaries and have an effect on the grain growth kinetics. Aluminum, sodium, titanium and iron were found on the surface and grain boundaries

* Corresponding author. Tel.: +41 44 633 6480; fax: +41 44 632 1132.
E-mail address: barbara.scherrer@mat.ethz.ch (B. Scherrer).

0378-7753/$ – see front matter © 2011 Elsevier B.V. All rights reserved.
doi:10.1016/j.jpowsour.2011.03.077

of YSZ [21,23,24]. Cross-contaminations, for example of alumina, are known to accelerate the grain growth due to sequestration of the silicon by the aluminum [26,27]. The impact of impurities like Si, Al and Mn on the electrical conductivity was investigated in bulk samples with different yttria contents [18,27–30]. Almost all impurities, alone or in combination, were found to increase the grain boundary resistivity. Silica at the electrode/electrolyte interface decreases the electrical performance [31–34]. It can be concluded from results from bulk YSZ that residual impurities such as silica strongly affect the microstructural evolution during heat treatments and tend to decrease overall electrical conductivity of the material.

The literature on silica as impurities in YSZ thin films is scarce. Thin films are normally contaminated by the bulk YSZ ceramics used as target material in the thin film deposition processes or during post-deposition processes. In the second case, the impurities are already present in the as-purchased raw material. Zirconia-based and zirconia-related thin films deposited on Si-wafer and SiO_2 glass are summarized in Table 1 [35–39]. To the author's knowledge, Si as surface impurity on zirconia-based thin films deposited on other Si-based substrate materials was not investigated so far. Si is capable to diffuse from a blank Si-wafer to the zirconia-based thin film surface. This proceeds at temperatures as low as 330 °C in ZrO_2 thin films even for thicknesses of around 100 nm [38]. Hwang et al. investigated the bulk of an YSZ thin film by XPS and found no Si within a 450 nm thick CVD thin film after deposition at 750 °C [39]. In addition to silica diffusion, zirconium inter-diffusion into silicon was reported [40]. Hertz et al. investigated electrochemical performance of Pt electrodes on bulk and thin film YSZ samples [8]. They found a increased electrode conductance for low-temperature treated samples where no silicon was detected on the YSZ surface. This supports the suggestion of de Ridder et al. and others, that Si at the specimen surface or at the electrode–electrolyte interface decelerates or even inhibits the oxygen exchange reaction [21,31,32]. So far, it is unclear to which extent the electric performance is affected by the impurities in YSZ thin films.

The following conclusions can be drawn from literature for the role of silica: (i) silica lowers the grain boundary mobility and therefore the grain growth kinetics in YSZ bulk ceramics, (ii) it lowers the overall electrical conductivity of YSZ bulk ceramics, (iii) it is capable to diffuse from Si-based substrates to YSZ thin films surface for temperatures above 330 °C, (iv) it effects the electrical properties at the YSZ surface and at the electrode–electrolyte interface due to a higher electrode overpotential. In order to elucidate the secondary effects of Si on the electric transport for such film–substrate interfaces and film surfaces, profound chemical and microstructural investigations are indispensable.

We thus investigate the impact of Si-based and Si-free substrates on the microstructure and chemistry of spray pyrolyzed yttria-doped-zirconia thin films indicated in the following as YSZ and having the following composition $Zr_{0.85}Y_{0.15}O_{2-\delta}$. The annealed thin films were probed by TEM and XPS to gain knowledge on the silicon contamination, its chemical surrounding and/or in-depth distribution. Furthermore, suitable processing guidance for substrate choice, critical temperature range and processing design of MEMS-based devices are given.

2. Experimental

2.1. Thin film preparation

YSZ thin films were deposited by air-blast spray pyrolysis as reported earlier [41]. A precursor solution was pumped to a spray gun (Compact 2000KM, Bölhoff Verfahrenstechnik, Germany) with a liquid flow rate of 2.5 ml h^{-1} where it was atomized with 1 bar air pressure and sprayed on a heated substrate at 370 ± 5 °C. The spray pyrolysis precursor solution consisted of zirconium acetylacetonate (Alfa Aesar, 99% purity) and yttrium chloride hydrate (Alfa Aesar, 99.9% purity) dissolved in 80 vol% tetraethylene glycol (TEG, Aldrich, 99%), 10 vol% polyethylene glycol 600 (Fluka) and 10 vol% ethanol (Fluka, 99.9%). The total salt concentration was 0.05 mol l^{-1}. A molar ratio of Zr:Y = 85.2:14.8 was chosen to obtain a $Zr_{0.852}Y_{0.148}O_{2-\delta}$ film composition. For YSZ thin film deposition the following substrate materials were selected: (i) 500 μm Si_xN_y-coated Si wafers (EPFL Lausanne, Switzerland), (ii) SiO_2 quartz wafer (University Wafer, USA), (iii) fused SiO_2 wafer (University Wafer, USA), (iv) 500 μm SiO_2-coated Si wafer (University Wafer, USA) and (v) Si-free random orientated sapphire (Al_2O_3) single crystal (Stettler, Switzerland). The working distance between the spray nozzle and the hot plate was kept at 39 cm during all experiments. Spray time was adjusted to the targeted film thickness required for microstructure and chemical composition analysis to 100 min and 50 min, respectively. YSZ thin films were amorphous after deposition and were crystallized by subsequent annealing at 600 °C and 1000 °C in air with isothermal hold of 20 h and a heating and cooling rate at ±3 °C min^{-1}, respectively.

Further details on the spray pyrolysis method for YSZ film deposition [42,43], and crystallization of the originally amorphous spray pyrolysis films are given in [44].

2.2. Microstructures

Top-view microstructures of the thin films were characterized using scanning electron microscopy (FEG-SEM, Zeiss LEO Gemini 1530, Germany) with an in-lens detector. Prior to imaging, the thin films were coated with carbon in order to avoid charging and to allow imaging at higher resolutions.

The YSZ thin films were analyzed by X-ray diffraction (XRD, Brucker AXS D8 Advance). The setup was equipped with a copper radiation source operated at 40 kV and 40 mA with a $K_{\alpha 1}$–Ge monochromator. The average grain sizes <80 nm were determined by corrected full width at half maximum (FWHM) of the (1 1 1) XRD peak in accordance with the Scherrer equation [45]. For larger average grain sizes, the intercept lengths of grain sizes from SEM pictures with more than 300 grains were measured with Lince 2.4.2β software [46].

Transmission electron microscopy (TEM) investigations were performed on ion-milled thin films prepared as cross-sections. For each sample, a stack was formed with two facing film-covered substrates, which was then embedded in a Cu tube to act as a stabilizing ring. Slices of the cylinder were cut, ground, and dimpled to a nominal thickness of 20 μm, after which they were ion-milled to electron transparency with a Gatan precision ion polishing sys-

Table 1
Literature summary for silicon as impurities on thin films deposited on Si-based substrates.

Material	Deposition method	Film thickness [nm]	Annealing conditions	Substrate	Silicon (at the surface)	Reference
HfO_2	RF sputtering	<5	800 °C, 30 min	Si	Yes	[30]
YSZ	PLD	27	After deposition (25 °C)	Si	Yes	[31]
ZrO_2	ALCVD	40	930 °C, 2 min	Si	Yes	[32]
ZrO_2	SP	100	330–380 °C	SiO_2 glass	5.5 at%	[33]
YSZ	CVD	450	After deposition (750 °C)	Si	No (in the film)	[34]

tem (PIPS). The PIPS milled with two argon ion beams at 3.5 keV and 4.0° angle of incidence from the top and bottom. TEM and energy-filtered transmission electron microscopy (EFTEM) images were obtained using a Jeol 2200FS TEM/STEM microscope operated at 200 kV and equipped with an in-column Omega-type energy filter.

2.3. Chemistry

EFTEM was used in order to analyze the elemental distribution of Zr, Y, O and Si. The collection angle of the EFTEM images was ~25 mrad. The conventional three-window technique was used to obtain element specific images. Zero-loss (ZL) filtered images were recorded with a 15 eV energy slit. Zr, O and Si elemental maps were obtained from the Zr–$M_{4,5}$, O–K and Si–$L_{2,3}$ edges with 20, 30 and 10 energy slits, respectively. The EFTEM maps labeled as Zr(Y)–$M_{4,5}$ are indeed maps of both Zr and Y since the Zr–$M_{4,5}$ and Y–$M_{4,5}$ edges are separated by only 22 eV and it is not possible to differentiate their signals by EFTEM. Acquisition times were typically between 10 and 20 s.

The chemistry of the YSZ thin films was investigated by X-ray photoelectron spectroscopy (XPS), which was performed in a PHI Quantera SXM (ULVAC-PHI, Chanhassen, MN, USA). Survey spectra were collected with a beam-size of 200 μm and a power of 49.5 W in fixed-analyzer-transmission mode (FAT) using a pass-energy of 280 eV and a step size of 1 eV. On the basis of the survey spectra, the following detailed regions were acquired in the high-resolution mode: Zr 3d, Y 3d, Y 3p, O 1s, Si 2p and C 1s. For YSZ thin films deposited on Si_xN_y-coated Si wafer and sapphire single crystal additional N 1s and Al 2p were measured, respectively. Depending on the surface contamination detected in the survey spectra, the spectra of Na 1s, K 2p and F 1s were also collected. During the spectra acquisition, the neutralizer was used ($p = 10^{-6}$ Pa, 1.3 V, 20 μA) in order to compensate for sample charging and the spectra were further corrected with reference to adventitious aliphatic carbon at 285.0 eV. The residual pressure in the spectrometer was always below 5×10^{-7} Pa. The system was calibrated according to ISO 15472:2001 with an accuracy of ±0.1 eV.

The high-resolution spectra of the composition depth-profile were obtained with the same beam size, 55 eV pass energy and a step size of 0.1 eV (full-width-at-half-maximum (FWHM) of the peak height for Ag $3d_{5/2}$ = 0.71 eV). The depth-profiles were measured, for each substrate material and annealing condition, on three independent samples. Data acquisition (200 μm beam size, 55 eV pass energy) was alternated with Ar^+-ion sputtering (2 min at 3 kV, 3 mm × 3 mm) for 30 cycles corresponding to 60 min total sputter time. The relative sputter rate is plotted as second *x*-axes in Figs. 5 and 6, and was determined on a Si/SiO_2 reference sample with a known thickness from ellipsometric measurements [47]. The films of roughly 300 nm in film thickness were etched through during the depth profiling.

The detailed spectra were processed using CasaXPS software (V2.3.15, Casa Software Ltd., UK). Prior to fitting of the detailed XP-spectra, an iterated Shirley–Sherwood background subtraction was applied using a linear-least-square algorithm. The product of Gaussian and Lorentzian functions was used for curve fitting. The spectra acquired during the sputtering depth-profile were also processed with CasaXPS. The curve fitting procedure was applied only in the case of the silicon and nitrogen signals; for all the other detailed spectra, the whole area under each signal was used to calculate the composition. Each elemental intensity was corrected for the relative sensitivity factor calculated from the inelastic mean free path according to Seah and Dench [48,49], Scofield photoionization cross-section [50], the angular asymmetry factor [51] and the analyzer transmission function [52]. A detection limit for Si of 0.2 at% was estimated for the XPS under these analysis conditions. For as-deposited thin films the Si content at the surface and within the film was always lower than the detection limit.

3. Results

3.1. Microstructure

SEM top-view micrographs of spray pyrolyzed YSZ thin films on Si-based and Si-free substrate materials are shown in Fig. 1. The selected substrates were Si_xN_y-coated Si wafers, SiO_2 quartz wafer

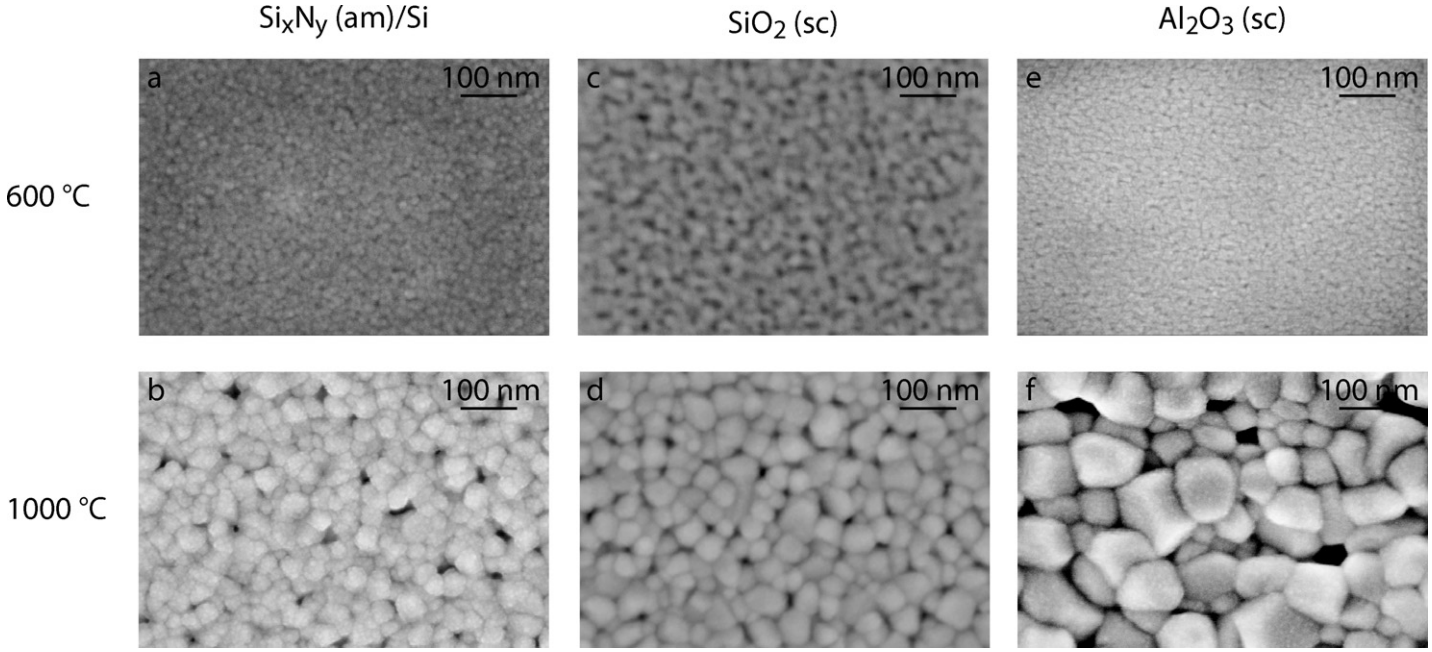

Fig. 1. Top-view SEM micrographs of spray pyrolyzed YSZ thin films deposited on different substrate materials and post-annealed at different temperatures (600 °C and 1000 °C for 20 h with heating and cooling rate at ±3 °C min^{-1}, respectively): (a, b) amorphous Si_xN_y-coated Si wafer, (c, d) SiO_2 single crystal and (e, f) sapphire single crystal. The abbreviations "am" and "sc" indicate the state of crystallinity of the substrate materials referring to "amorphous" and "single crystalline", respectively.

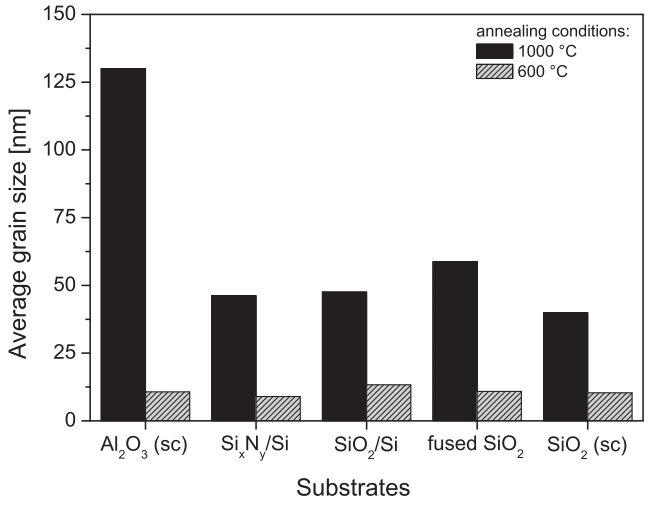

Fig. 2. Average grain size of YSZ thin films with respect to substrate materials and annealing conditions (600 °C and 1000 °C for 20 h with heating and cooling rates of ±3 °C min^{-1}).

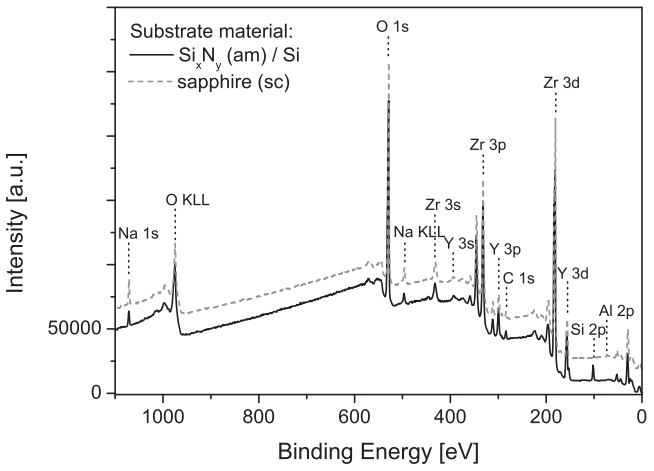

Fig. 3. XPS survey spectra of YSZ thin films deposited on amorphous Si_xN_y-coated Si wafer (filled line) and sapphire singe crystal (dotted line), respectively. Both films were previously annealed at 1000 °C for 20 h with a heating and cooling rate of ±3 °C min^{-1}.

and sapphire. The displayed microstructures are from thin films after an isothermal hold at 600 °C and 1000 °C for 20 h. All thin films were crack-free and show microstructures with a continuous network of neighboring grains after post-annealing.

The average grain sizes were determined by XRD and SEM and are summarized in Fig. 2. For the films annealed at 600 °C, a grain size of 11 ± 5 nm (XRD) independent on the substrate material was measured. A temperature increase up to 1000 °C results in average grain sizes of 48 ± 10 nm (XRD) and 130 ± 50 nm (SEM) for the Si-containing substrates and Si-free sapphire, respectively. Hence, the average grain size is about 2.5 times larger for the Si-free sapphire substrate compared to Si-based substrates. The SEM top-views show in case of films annealed at 1000 °C intergranular pores independent on the substrate material.

The substrate material affects the microstructures of YSZ films after annealing at 1000 °C. Si-based substrate materials lower the average grain size of the YSZ thin films.

3.2. Chemistry

The XPS survey spectra for YSZ thin films were taken to detect impurities and to allocate the exact peak positions for the high-resolution spectra. The spectra for the YSZ thin films deposited on amorphous Si_xN_y-coated Si wafer and sapphire, annealed at 1000 °C for 20 h are shown exemplarily in Fig. 3. The films were isothermally annealed at 1000 °C for 20 h before measurement. In the spectra of the thin film deposited on Si_xN_y-coated Si wafer and single crystalline sapphire, strong signals were found for Zr 3s, 3p and 3d, Y 3p and 3d, O 1s and KLL as well as C 1s. The Si 2p signal at ca. 101 eV was strong for Si-based substrate material and weak for sapphire. An additional Al 2p contribution was measured on the YSZ films deposited on sapphire. Sodium, potassium, fluorine and nitrogen impurities were additionally detected on the surfaces of some thin films.

In Fig. 4, high-resolution XP-spectra for the elements Zr, Y, O and Si are shown exemplarily for the YSZ thin films deposited on Si_xN_y-coated Si wafer and post-annealed at 600 °C and 1000 °C for 20 h, respectively. The spectra collected on the pristine thin film surface (full line) and after 120 s of Ar^+-sputtering (dotted line) (equals to about 20 nm) into the film are shown. The high-resolution XP-spectra for Zr 3d (Fig. 4a) at the surface of the low-temperature annealed sample show the typical peak duplet for the $3d_{5/2}$ and $3d_{3/2}$ [53,54]. Duplet splitting is around 2.5 eV and the area ratio is 3:2 for $d_{5/2}$:$d_{3/2}$. This is in agreement with literature [53,54]. During Ar^+-sputtering the shape of the well separated peak duplet changes. Both peaks get broader and less intense; at the lower energy side a large shoulder appears due to the preferential sputtering of the oxygen and therefore the partial reduction of the zirconium [55]. The high-temperature annealed sample shows the same peak position and sputtering effects as the low-temperature annealed thin film. Two pronounced and one very weak peaks are visible in the high-resolution Y 3d spectra between 147 eV and 164 eV at the surface of the YSZ thin film post-annealed at 600 °C for 20 h (Fig. 4b). The two peaks above the 156 eV binding energy are Y $3d_{5/2}$ and Y $3d_{3/2}$ with an area ratio of 3:2 [54]. In addition to these peaks, a very small Si 2s peak was found at 153.1 eV. After sputtering, the Y 3d peaks get broader and the Si 2s signal vanishes. For the 1000 °C post-annealed YSZ thin film, the Y 3d peaks are similar to the low-temperature annealed sample whereas at the surface of the YSZ thin film the Si 2s peak at 154.1 eV is much more pronounced. The Si 2s peak disappears after one Ar^+-sputtering cycle. The calculation of the Y-content for the depth-profiles is thus based on the Y 3p area. In the oxygen high-resolution spectra two oxygen species with different chemical environments were detected for both annealing temperatures (Fig. 4c). For the low-temperature sample, a distinctive O 1s signal at 530.2 ± 0.2 eV was found, which corresponds to oxygen in YSZ and is denoted as O–Zr(Y) [53]. On the high binding energy side of the O–Zr(Y) peak a shoulder is visible at 531.8 ± 0.2 eV. According to Riehl-Chudoba et al. this is related to oxygen bound to silicon [56]. After Ar^+-sputtering the O–Si shoulder disappears. For the 1000 °C annealed YSZ thin film, a similar situation was measured whereby the O 1s signal assigned to O–Si at the surface is more pronounced. The Si 2p signal consists of a peak duplet of Si $2p_{3/2}$ and Si $2p_{1/2}$ with an area ratio of 2:1 = Si $2p_{3/2}$:Si $2p_{1/2}$ and a splitting of 0.8 eV (Fig. 4d). The low-temperature annealed YSZ thin film exhibited a small Si 2p double peak with the centroid at 103.0 ± 0.3 eV. This may be assigned to silicon in a Si–O–Zr component as reported by Giustino et al. and Gutowski et al. [57,58]. Its binding energy is about 1 eV lower compared to SiO_2 due to the lower electron negativity of zirconium compared to silicon. For the high-temperature annealed YSZ thin film, a more pronounced Si–O–Zr peak duplet at 101.8 ± 0.2 eV was measured. After sputtering, the intensity of the Si 2p duplet found at the surface of the sample decreased and for high amounts of Si–O–Zr, a new peak at lower binding energy of ca. 97.5 eV appears. This new peak is due to the preferred sputtering of oxygen and therefore its reduction from Si–O–Zr to Si or an intermedi-

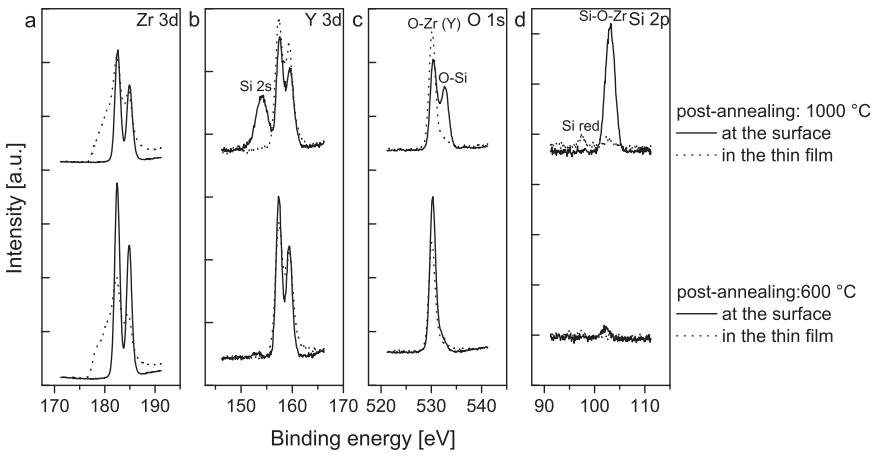

Fig. 4. XPS high-resolution spectra of Zr 3d, Y 3d, O 1s and Si 2p measured at the surface of YSZ thin film (filled line) and in the thin film, i.e. after Ar^+-sputtering for 120 s into the thin films (dotted line). Thin films were deposited on amorphous Si_xN_y-coated Si wafers and annealed at 600 °C and 1000 °C for 20 h with heating and cooling rates of ±3 °C min^{-1}, respectively. In Fig. 4d, elemental silicon is denoted as "Si red".

ate state. For the sake of simplicity these are not displayed in Figs. 5 and 6.

All films in this study revealed an atomic ratio of Zr:Y = 86.0 ± 0.5:14.0 ± 0.5 over the entire film thickness independent on the annealing conditions and underlying substrate material. This is in agreement with the desired film composition of 14.8 at% yttrium doping in the host lattice. The concentration was calculated by averaging the concentration in the steady state region of the thin film.

The chemical composition of the substrate was determined via XPS and is summarized in Table 2. The signal denoted as Si–N is assigned to silicon neighbored by up to four nitrogen atoms, the binding energy being 101.6 eV. The Si content of the Si_xN_y coating was found to be 57.0 ± 0.9 at% which is higher than the expected value of 42.9 at%. This finding might be explained by the fact that the Si_xN_y coating was designed to have a low stress level within the layer which can be achieved via a higher Si content than stoichiometrically needed [59,60]. Additionally, the nitrogen is preferentially sputtered compared to silicon. The second explanation also holds for the other two substrate materials. In both cases, a higher silicon and aluminum content as the theoretical one for SiO_2 and Al_2O_3 were measured, respectively.

The analysis of the high-resolution spectra was the base for the calculation of the atomic ratios of chemical elements during Ar^+-etching of the YSZ thin films with respect to substrate materials for the XPS depth-profiles in Figs. 5 and 6 for low- and high-annealing temperatures, respectively. In general, there are four main regions visible in all the profiles: (i) the surface of the YSZ thin films, (ii) the thin film itself, (iii) the thin film–substrate interface, and (iv) the substrate material after a sputtering time of 960–3000 s. In order to simplify the XPS depth-profiles all impurities including carbon are not shown in Figs. 5 and 6 as they were only detectable at the pristine surface. For this reason the atomic percent do not sum up to 100 at%.

Table 2
The measured elemental ratio of the substrate materials measured by XPS compared to the theoretical ones.

Substrate material	Measured elemental ratio [%]		Theoretical elemental ratio [%]	
	Si or Al	N or O	Si or Al	N or O
Si_xN_y (am)/Si	57.0 ± 0.9	43.0 ± 0.9	43	57
SiO_2 (single crystal)	40 ± 2	60 ± 2	33	67
Sapphire (single crystal)	46 ± 1	55 ± 1	40	60

In the following, the results from the films annealed at 600 °C are presented (Fig. 5). The *YSZ thin film deposited on Si_xN_y-coated Si wafer* contains mainly oxygen, zirconium and yttrium (Fig. 5a). At the surface, the oxygen content is about 10 at% higher than in the thin film which is caused by the preferential etching of the oxygen compared to metal ions. Additional 1.7 at% silicon mainly as Si–O–Zr was detected at the surface which drops below the detection limit of 0.2 at% in the YSZ. The Si–O always stays below the detection limit. For *YSZ thin films on single crystalline SiO_2* a very similar Si–O–Zr surface concentration of 1.2 at% was measured which drops below the detection limit within the YSZ (Fig. 5b). Compared to the YSZ on the Si_xN_y, oxygen does not decrease along with the zirconium and yttrium content; it is increasing due to the higher oxygen content within the substrate material. For the *YSZ thin film deposited on a sapphire single crystal* (Fig. 5c), the Si–O–Zr content measured at the surface is with 0.6 at% only half the amount compared to the surface concentration on Si-based substrates. In addition to the silicon, 0.9 at% aluminum was detected at the YSZ surface and 1.3 at% within the YSZ thin film. The aluminum content starts to increase drastically after a sputter time of 960 s and reaches a stable value after 3000 s of sputtering.

Fig. 6 shows the concentration depth-profiles of YSZ thin films post-annealed at 1000 °C for 20 h. The depth-profile of *YSZ thin film deposited on Si_xN_y-coated Si wafer* is displayed in Fig. 6a. The silicon Si–O–Zr signal with 11 at% is clearly observable at the surface. In the low-temperature annealed sample, this silica concentration is much lower (1.7 at%). A rather high concentration of about 3 at% of Si–O–Zr was measured within the high-temperature annealed YSZ thin film. At the interface between the YSZ film and the substrate material, a high silicon concentration assigned as Si–O was detected. In all the other depth-profiles no interfacial reaction was observed. The depth-profile for the *YSZ thin film deposited on single crystalline SiO_2* annealed at 1000 °C for 20 h is displayed in Fig. 6b. The profile looks similar to the one annealed at 600 °C, except the Si–O–Zr concentration is higher by a factor of 7 at the YSZ surface. Within the thin film the Si–O–Zr concentration is 1.1 at%. For the *YSZ thin films deposited on sapphire* (Fig. 6c), the silicon and aluminum concentrations on the films surfaces are 1.3 at% and around 2 at%, which in both cases is about doubled compared to the films annealed at 600 °C. The aluminum content at the surface and within the YSZ thin film is the same. Table 3 summarizes the Si- and Al-concentrations. It can be concluded that silicon diffuses from Si-based substrates, e.g., amorphous Si_xN_y-coated Si wafer or single crystalline SiO_2, towards the surface of YSZ thin films for temperatures as low as 600 °C. This effect is more pro-

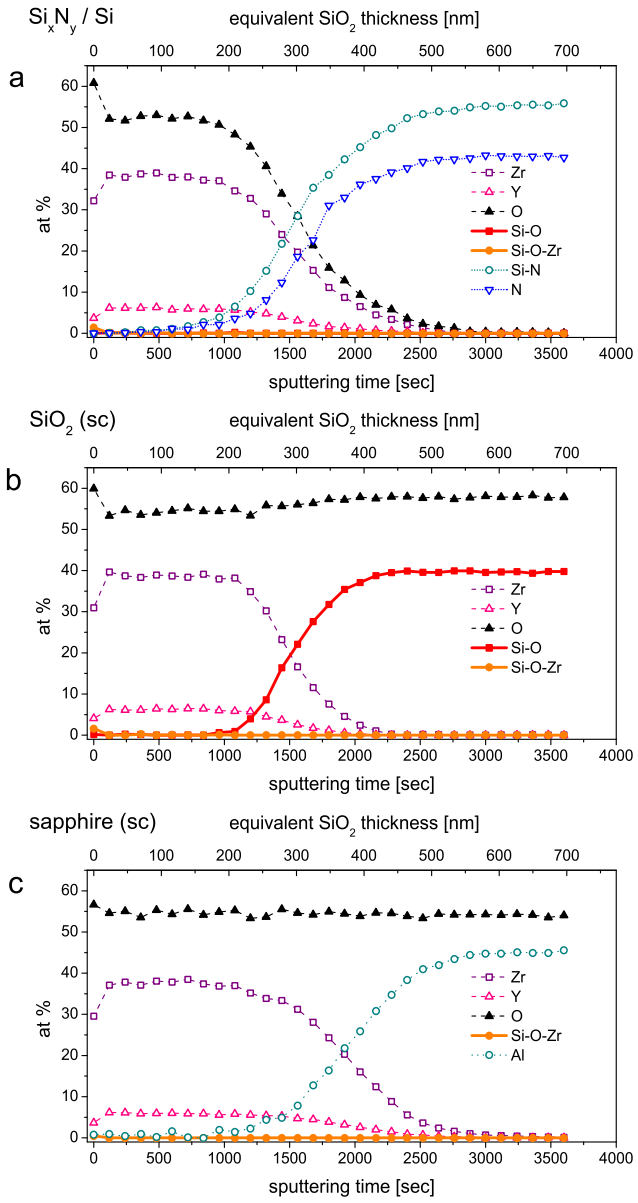

Fig. 5. XPS depth-profiles of spray pyrolyzed YSZ thin films post-annealed at 600 °C for 20 h on different substrates: (a) amorphous Si_xN_y-coated Si wafer, (b) SiO_2 single crystal, and (c) sapphire single crystal. Films were always heated and cooled at ±3 °C min^{-1}.

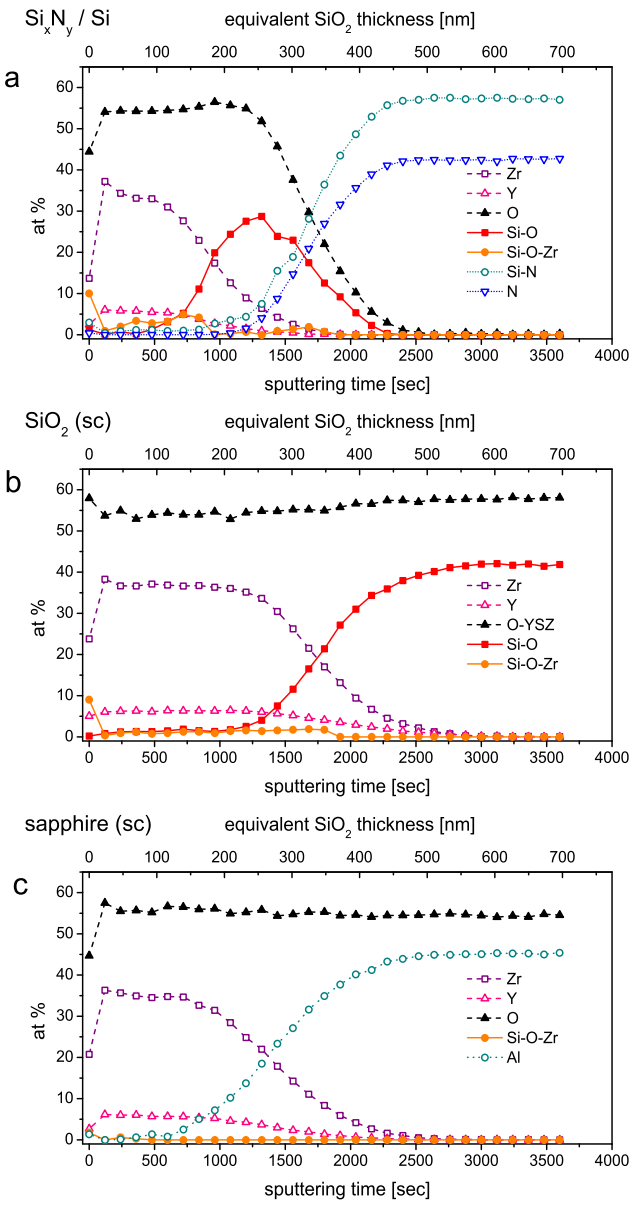

Fig. 6. XPS depth-profiles of spray pyrolyzed YSZ thin films post-annealed at 1000 °C for 20 h on different substrates: (a) amorphous Si_xN_y-coated Si wafer, (b) SiO_2 single crystal, and (c) sapphire single crystal. Films were always heated and cooled at ±3 °C min^{-1}.

nounced for further thermal activation. Up to 8–11 at% of Si was found on the YSZ film surface after 1000 °C for 20 h. For all YSZ thin films no interface reaction between the YSZ and the substrate material could be detected, except for the YSZ thin film deposited on Si_xN_y and annealed at 1000 °C for 20 h. Here Si–O species were detected.

3.3. TEM analysis

The YSZ thin films on the Si-based substrates were analyzed in the TEM and by elemental mapping. In the sample deposited on amorphous Si_xN_y-coated Si wafer post-annealed at 600 °C for 20 h, the YSZ thin film is 187 nm thick with a grain size gradient from

Table 3
Si and Al content measured by XPS at the surface and in the YSZ thin films with respect to the substrate material and annealing conditions. The standard deviations were calculated averaging over three independent measurements.

Impurity	Substrate material	600 °C for 20 h Content [at%]		1000 °C for 20 h Content [at%]	
		At the surface	In the thin film	At the surface	In the thin film
Silicon	Si_xN_y (am)/Si	1.7 ± 0.9	<0.2	10.5 ± 2.9	2.9 ± 2.0
	SiO_2 (single crystal)	1.2 ± 0.6	<0.2	8.7 ± 0.5	1.1 ± 0.2
	Sapphire (single crystal)	0.6 ± 0.3	<0.2	1.3 ± 0.9	<0.2
Aluminum	Sapphire (single crystal)	0.9 ± 0.1	1.3 ± 1.0	2.2 ± 0.8	2.1 ± 0.4

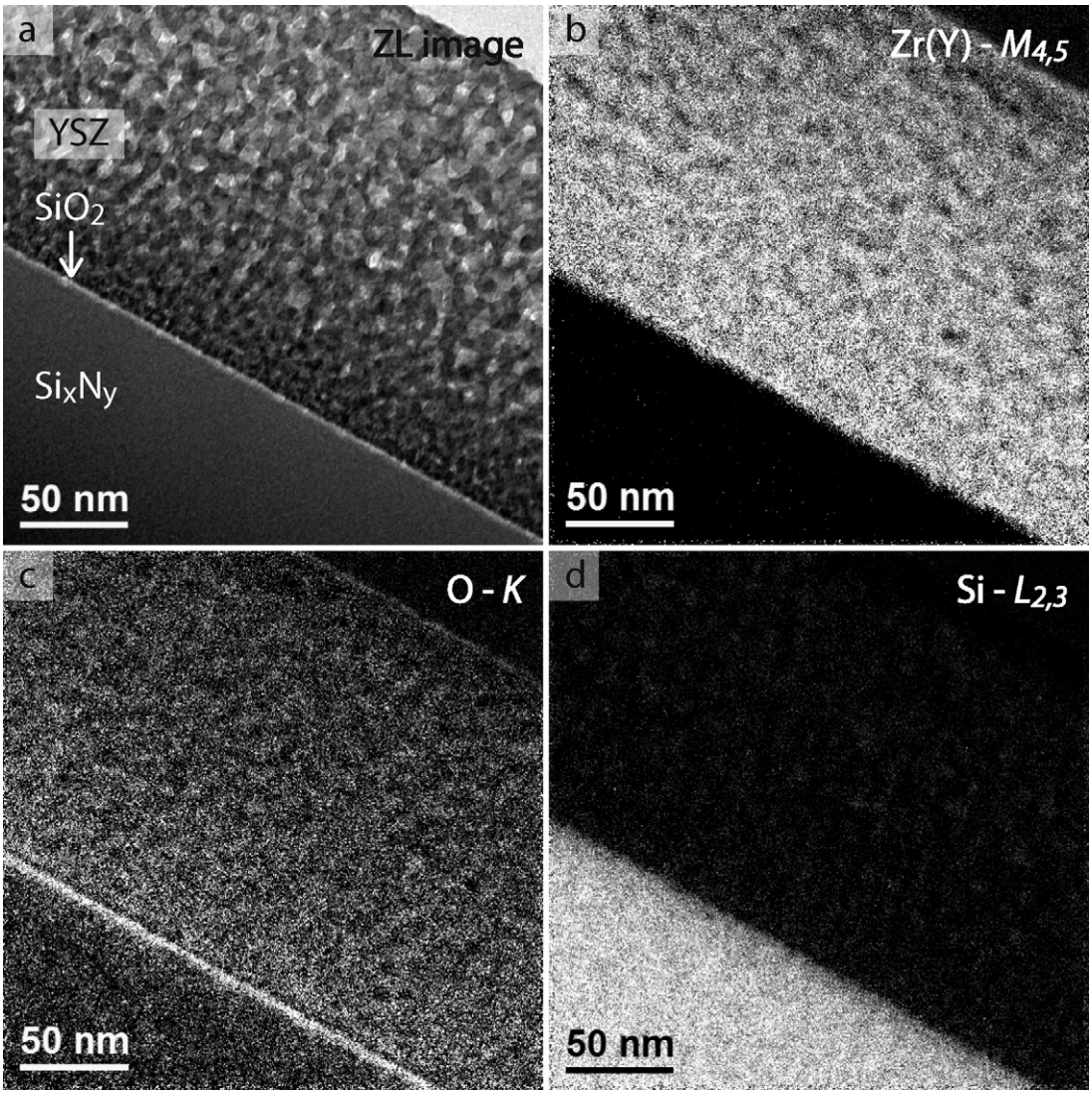

Fig. 7. Energy-filtered transmission electron micrographs (EFTEM) of spray pyrolyzed YSZ thin films deposited on amorphous Si_xN_y-coated silicon wafer and annealed at 600 °C for 20 h: (a) zero loss (ZL) image, (b–d) elemental maps of Zr, O, and Si, respectively.

the interface to the surface from 3 nm to 10 nm in average (Fig. 7a). The brightness in the zero loss (ZL) image correlates with the density of the detected material. The ZL image indicates by the bright spots between neighboring grains, that the YSZ film has intergranular pores, which were confirmed by STEM (not shown here). The pores within the YSZ thin film are in the same size range as the grains and show a similar gradient over the cross-section of the thin film. Between the YSZ and the 494 nm thick Si_xN_y substrate coating, a layer was found with a thickness of 3 nm. According to electron diffraction this layer is amorphous. In the elemental map the image intensity scales linearly with the concentration of the mapped element. The Zr/Y map shows a variation of the brightness within the YSZ thin film (Fig. 7b). The oxygen is present in the YSZ film enriched within the amorphous layer at the YSZ–Si_xN_y interface (Fig. 7c). The Si has a very low but non-uniform disposition within the YSZ film, and a higher and uniform content in the amorphous interfacial layer and the Si_xN_y coating (Fig. 7d). We conclude that the detected amorphous layer at the interface between the YSZ thin film and the Si_xN_y coating consists mainly of SiO_2.

In Fig. 8, the energy-filtered transmission micrographs are shown for an YSZ thin film deposited on Si_xN_y-coated Si wafer and post-annealed at 1000 °C for 20 h. The film thickness is 122 nm with a grain size in the range of 15 nm to 55 nm (Fig. 8a). The bright areas are pores within the YSZ thin film. A porosity of 10–20 vol% was confirmed by additional STEM images not shown in this study. As for the sample annealed at 600 °C, an amorphous layer of SiO_z (65 nm) was detected between the YSZ thin film and the amorphous Si_xN_y coating. This is in agreement with the sputter depth-profile (Fig. 6a). The Si_xN_y coating has a thickness of 454 nm. The combined Zr and Y map shows an uneven distribution of the elements within the YSZ layer (Fig. 8b). The oxygen content of the YSZ thin film is lower than within the amorphous layer below (Fig. 8c). The silicon shows brighter areas in the YSZ thin film where the Zr/Y map shows depletion (Fig. 8d). We conclude that the Si is accumulated at the grain boundaries of the YSZ grains. The Si signal is pronounced within the amorphous 65 nm thick layer and a residual brightness was found for Zr/Y as well. Like the very thin amorphous layer detected in the 600 °C annealed sample, the 65 nm thick layer at the interface between the YSZ thin film and the Si_xN_y coating consists mainly of SiO_2. In the case of the sample annealed at 1000 °C, additional small amounts of Zr and Y were observed within this layer (Fig. 8b).

The YSZ thin film deposited on SiO_2 and post-annealed at 600 °C for 20 h is shown in Fig. 9. In the zero loss image of the YSZ, a similar grain and pore size gradient as in the thin film deposited on Si_xN_y is visible (Fig. 9a). On top of the YSZ layer a residual resist is visible. For the TEM lamella preparation, the samples were imbed-

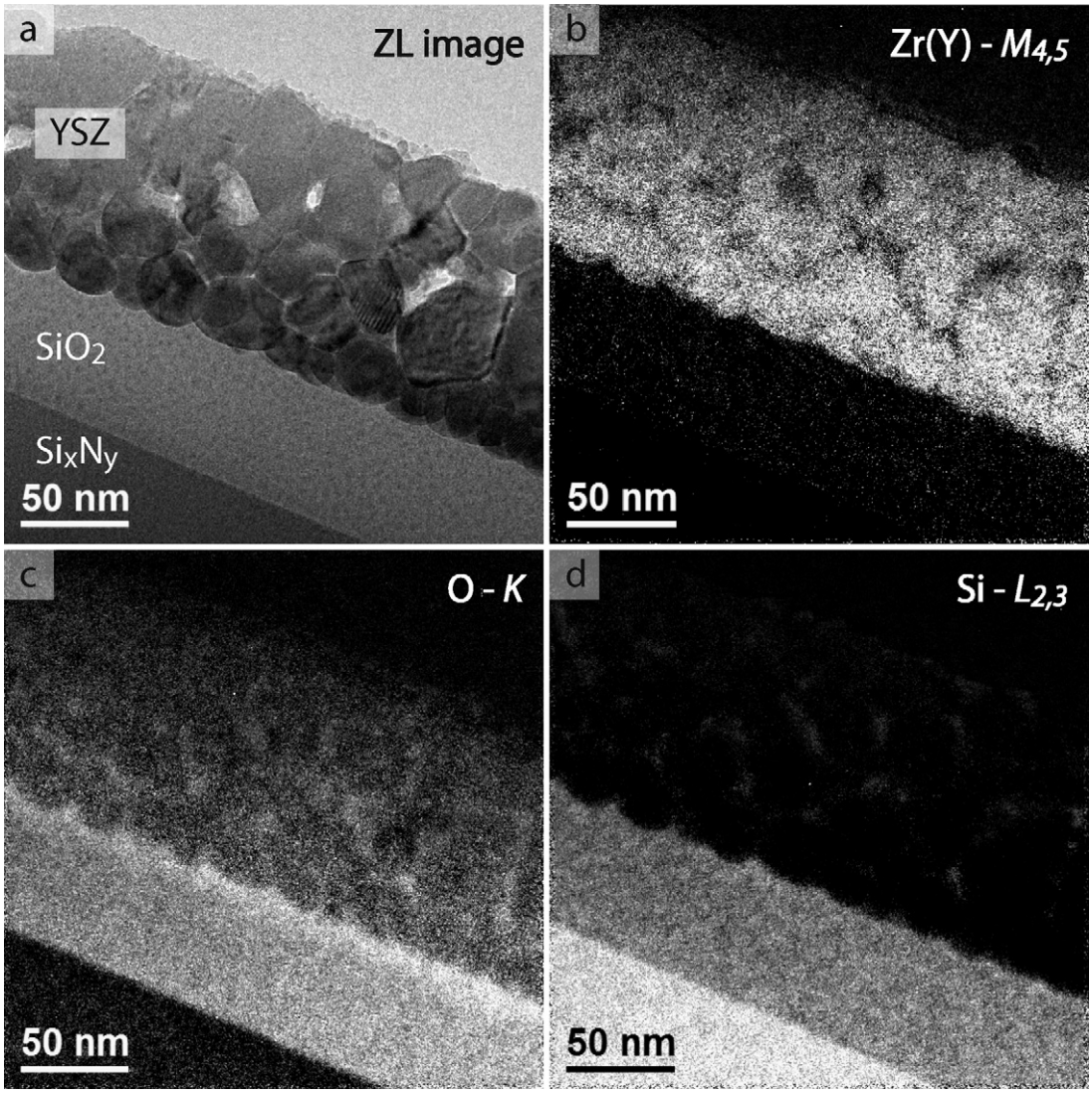

Fig. 8. Energy-filtered transmission electron micrographs (EFTEM) of spray pyrolyzed YSZ thin films deposited on amorphous Si_xN_y-coated silicon wafer and annealed at 1000 °C: (a) zero loss (ZL) image, (b–d) elemental maps of Zr, O, and Si, respectively.

ded with resist which was removed via ion milling in some areas. A comparable picture for the elemental maps was measured with a non-uniform distribution of Zr and Y, respectively. The Si content varies within the YSZ thin film and has a higher content at the surface and at the YSZ thin film grain boundaries. The oxygen map shows a higher concentration in the substrate material than in the YSZ thin film.

In Fig. 10, an YSZ thin film deposited on single crystalline SiO_2 and annealed at 1000 °C for 20 h is shown. The YSZ thin film thickness varied drastically with the position due to the high surface roughness of spray pyrolysis films. The images were taken at a film position with a low thickness. On the top of the YSZ thin film residual resist is visible. The grain size is between 10 nm and 40 nm. The pores size is in the same range as the grain size. As in the YSZ on Si_xN_y, the Zr(Y) map shows depleted areas in the YSZ on SiO_2 single crystal where an accumulation in the Si map was measured. We thus conclude that the Si is located at the grain boundaries of the YSZ grains. The oxygen content is lower in the YSZ thin film than in the SiO_2 substrate material.

The TEM results show that silica persists at the grain boundary in the YSZ thin films. For the YSZ thin films deposited on Si_xN_y-coated Si wafer the interface is oxidized to SiO_z even for low-temperature annealing of 600 °C for 20 h.

4. Discussion

4.1. Silicon on and in the YSZ thin films

All films deposited on Si_xN_y-coated Si wafers and SiO_2 quartz wafers reveal for temperatures at 1000 °C for 20 h significant Si concentrations of 8–11 at% on the surface of the YSZ thin films. Since the low-temperature YSZ films show lower Si surface contents of 1.5 at% on the YSZ films, the Si diffusion process is thermally activated. Si-diffusion has to be accounted for all YSZ films operated in Si-based MEMS devices – even for temperatures as low as 600 °C. In the literature, silicon was detected on the surface; however, the annealing times were short (30 min) and the film thicknesses of 5–40 nm were much smaller compared to the films in this study [35–37]. Literature results tend in the same direction as the ones presented here. Peshev et al. found 5.5 at% Si after 330–380 °C at the surface of a 100 nm thick YSZ thin film [38]. However in this study the as-deposited thin films at 370 °C showed no Si contamination. According to TEM analysis, Si is preferentially concentrated at the grain boundary of the YSZ films. It is known from literature on sintered bulk pellets that silicon preferably stays at the grain boundary of YSZ compared to the grain interior due to the low solubility of the Si in zirconia [17]. This is visible in the TEM images in

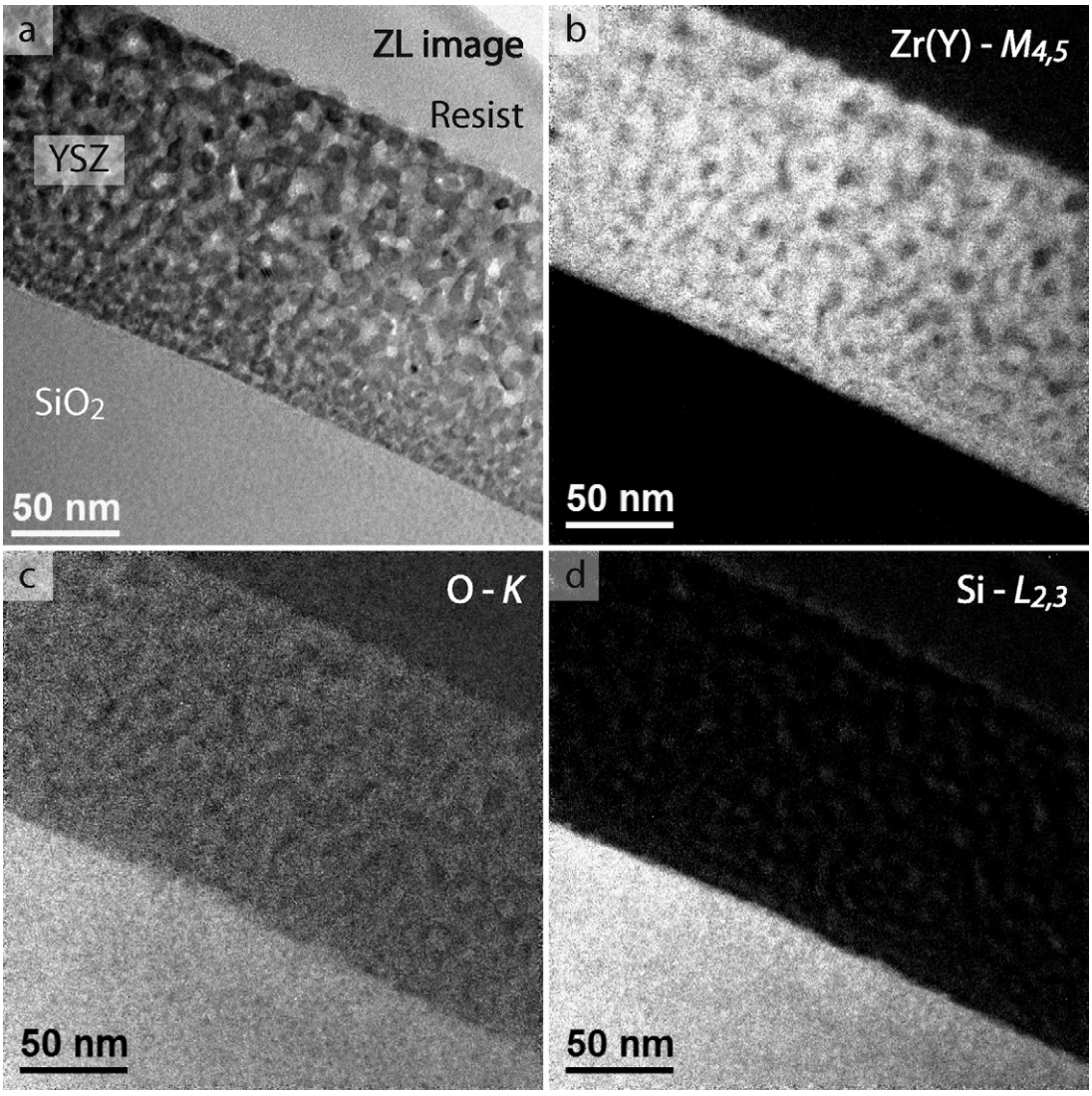

Fig. 9. Energy-filtered transmission electron micrographs (EFTEM) of spray pyrolyzed YSZ thin films deposited on singe crystal SiO_2 wafer and annealed at 600 °C for 20 h: (a) zero loss (ZL) image, (b–d) elemental maps of Zr, O, and Si, respectively.

Figs. 8 and 10 where the samples annealed at 1000 °C for 20 h are shown.

If we compare the silicon content with respect to the substrate materials, we observe the highest amount of Si for the amorphous Si_xN_y-coated Si wafer (Table 3). This could be explained by the lower thermodynamic stability of Si_3N_4 compared to SiO_2 in air [61]. In the case of sapphire, the low Si surface concentration of maximal 1.3 at% after 1000 °C for 20 h is most likely due to the silicon contaminations from the furnace [24]. This processing-related silicon content is always present on the silicon-based substrate materials and can be subtracted from actual amounts.

4.2. Chemical analysis of the interface between YSZ thin film and substrate material

During the post-annealing of the thin films, the interface was stable for the single crystal sapphire and the single crystal SiO_2 substrate material as shown by the XPS depth-profile and by the TEM analysis. The Si_xN_y-coated Si wafers were oxidized at the interface between the coating and the YSZ thin film for both temperatures (Figs. 6a, 7 and 8). An amorphous SiO_z layer was built with a thickness of 3 nm and 65 nm after annealing at 600 °C and 1000 °C for 20 h, respectively. Looking at the binding energy shift in the high-resolution XP-spectra, we conclude that this SiO_z layer is almost stoichiometric and only very small amounts of zirconium and or yttrium are dissolved within the layer [58,62]. We conclude that the SiO_z layer was formed at the expenses of the Si_xN_y coating and not of the YSZ. This is supported by the lower silicon nitride thickness of 454 nm after 1000 °C instead of the original 500 nm. The small amounts of Zr(Y) are not surprising as Zr is known for its high diffusivity within Si [40]. This is in agreement with the thermodynamic stability of Si_3N_4, which oxidizes to SiO_2 at 1000 °C and for oxygen partial pressures higher than 10^{-17} Pa [61]. However, no literature data was found for temperatures as low as 600 °C, whereas a 3 nm thick SiO_z layer was detected in this study.

4.3. Microstructure of the YSZ thin films

For the YSZ thin films on the Si-containing substrate materials, a 2.5 times smaller grain size was measured compared to films on sapphire substrates for an isothermal hold of 20 h at 1000 °C (Figs. 1 and 2). This difference in grain size dependent on the substrate material for 1000 °C is related to the Si impurities lowering the grain boundary mobility in the YSZ films [17–24]. In the 600 °C post-annealed samples, no impact of the Si-impurities on grain growth is detectable. Independent on the substrate material, simi-

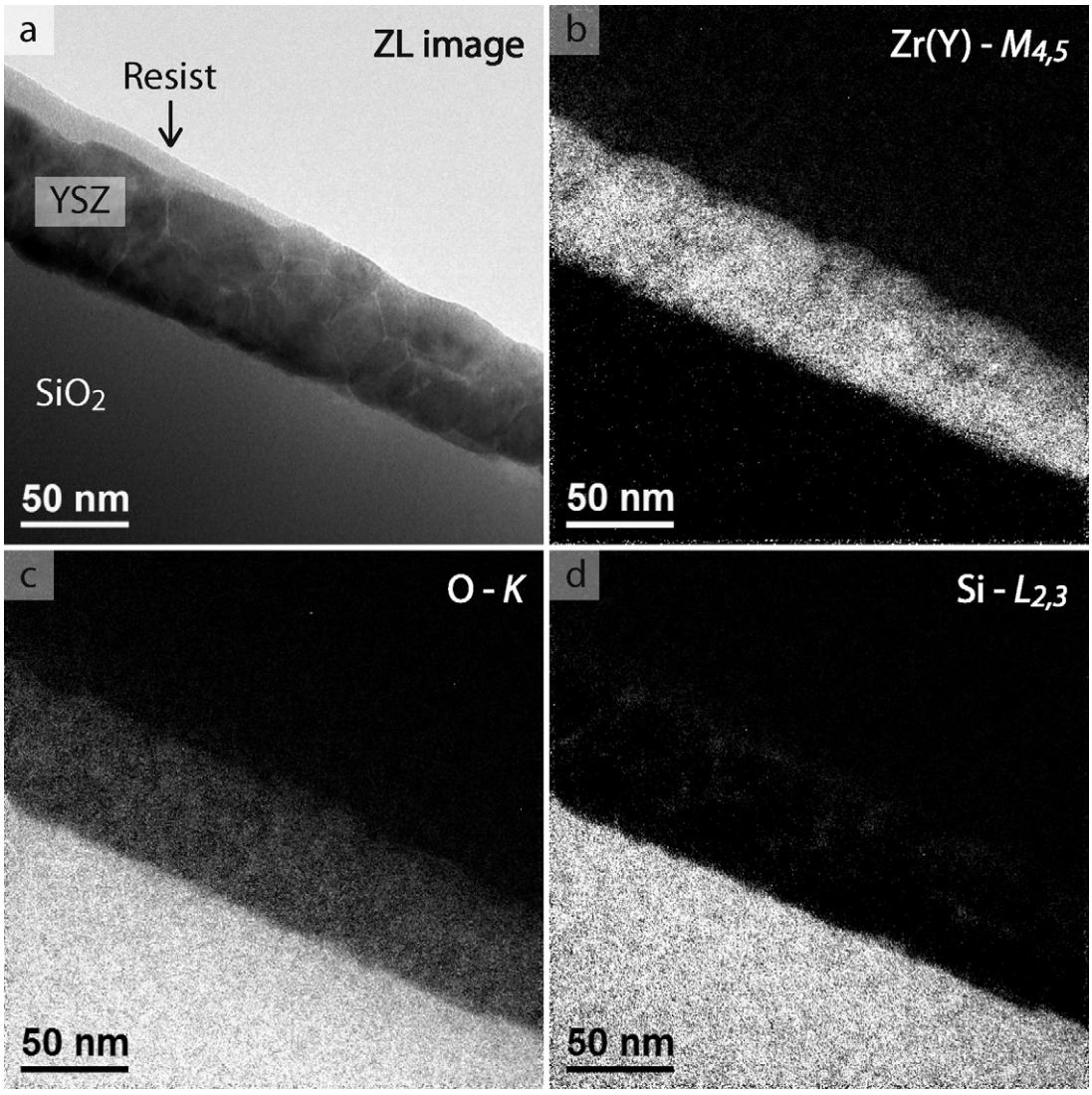

Fig. 10. Energy-filtered transmission electron micrographs (EFTEM) of spray pyrolyzed YSZ thin films deposited on a singe crystal SiO_2 wafer and annealed at 1000 °C for 20 h: (a) zero loss (ZL) image, (b–d) elemental maps of Zr, O, and Si, respectively.

lar grain sizes are measured. Interestingly, a grain size gradient was observed for the low-temperature annealed samples (Figs. 7 and 9). This gradient could be due to the small (<0.2 at%) but still present Si concentration within the thin films which becomes larger closer to the substrate [17,18,27,63]. This hypothesis is supported by the cross-section of an YSZ thin film deposited on sapphire and annealed for 20 h at 600 °C where no grain size gradient was observed (not shown here).

4.4. Aluminum on and in the YSZ thin films

For the YSZ thin films deposited on sapphire single crystal, additional alumina was found as impurity. The Al diffused into the YSZ thin film and the Al from the substrate could not be separated as the peak position gradually sifted from 73.8 eV to 75.6 eV binding energy during sputtering [64,65]. If we have a closer look at the Al amount found at the surface and within the YSZ, we observe that the aluminum concentration is almost the same, around 1 and 2 at% for a post-annealing at 600 °C and 1000 °C, respectively. This leads to the conclusion that in contrast to Si – where the surface concentration was always higher – Al dissolves comparably well in the grain interior and the grain boundary. In literature, however, alumina (>3 wt%) was found to segregate to the grain boundary and sequestrate there silicon impurities [29,66,67]. Though Hughes et al. have pointed out that this reaction requires high temperatures (»1000 °C) [66].

5. Conclusion

Diffusion of Si from the Si-based substrates into the grain boundaries of the YSZ thin film and to its surface was observed for annealing temperatures as low as 600 °C.

A silicon content of 3 at% was found in the bulk of the thin film deposited on the Si_xN_y-coated substrate after annealing at 1000 °C. At the surface of the thin film, the Si concentration was 11 at%. This is higher compared to the thin film deposited on SiO_2 single crystal due to the ease of diffusivity depending on the thermal stability and crystal structure of the substrate. The diffusion of Si into the material affects the grain size of the YSZ thin film. For samples annealed at 1000 °C for 20 h, the grain size changes from about 50 nm for the Si-based to 130 nm for the Si-free substrate materials. This difference by a factor of 2.5 can be explained by the Si, which is located at the grain boundaries and acts as grain boundary pinning agent. Despite that no grain size dependency on the substrate material was found for the YSZ thin films annealed at 600 °C, two times higher Si concentration was detected via XPS on

films deposited on Si-based substrates, compared to the films on sapphire.

Therefore, even for a temperature as low as 600 °C, it is important to design the process route for Si-based substrates, sealing- and housing-components according to the Si sensitivity of the final device. In order to lower the possibility for silicon diffusion into the active area of an electrochemical device, such as e.g. a micro-SOFC, one should aim for processing and operating temperatures lower than 600 °C or do heat treatment without a substrate below functional layers, i.e. heat treatment only after free-standing membrane fabrication.

Acknowledgment

The authors thank Anna Evans for stimulation discussions. Financial support by the following Swiss institutions is gratefully acknowledged:

- Center of Competence Energy and Mobility (CCEM) within the framework of the ONEBAT project.
- Competence Centre for Materials Science and Technology (CCMX) within the framework of the NANCER project.
- Swiss Electric Research (SER) within the framework of the ONEBAT project.
- Swiss National Foundation (SNF) within the framework of the Sinergia project ONEBAT.

References

[1] S.J. Skinner, J.A. Kilner, Materials Today 6 (2003) 30.
[2] J.W. Judy, Smart Materials & Structures 10 (2001) 1115.
[3] A. Evans, A. Bieberle-Hütter, H. Galinski, J.L.M. Rupp, T. Ryll, B. Scherrer, R. Tölke, L.J. Gauckler, Chemical Monthly – Monatshefte der Chemie Monatsh Chem (2009).
[4] A. Evans, A. Bieberle-Hütter, J.L.M. Rupp, L.J. Gauckler, Journal of Power Sources 194 (2009) 119.
[5] A. Bieberle-Hütter, D. Beckel, A. Infortuna, U.P. Muecke, J.L.M. Rupp, L.J. Gauckler, S. Rey-Mermet, P. Muralt, N.R. Bieri, N. Hotz, M.J. Stutz, D. Poulikakos, P. Heeb, P. Müller, A. Bernard, R. Gmür, T. Hocker, Journal of Power Sources 177 (2008) 123.
[6] U.P. Muecke, D. Beckel, A. Bernard, A. Bieberle-Hutter, S. Graf, A. Infortuna, P. Muller, J.L.M. Rupp, J. Schneider, L.J. Gauckler, Advanced Functional Materials 18 (2008) 3158.
[7] S.J. Litzelman, J.L. Hertz, W. Jung, H.L. Tuller, Fuel Cells 8 (2008) 294.
[8] J.L. Hertz, A. Rothschild, H.L. Tuller, Journal of Electroceramics 22 (2009) 428.
[9] E. Traversa, The Electrochemical Society Interface 18 (2009) 49.
[10] Z. Shao, S.M. Haile, J. Ahn, P.D. Ronney, Z. Zhan, S.A. Barnett, Nature 435 (2005) 795.
[11] H. Huang, M. Nakamura, P.C. Su, R. Fasching, Y. Saito, F.B. Prinz, Journal of the Electrochemical Society 154 (2007) B20.
[12] J.H. Shim, C.-C. Chao, H. Huang, F.B. Prinz, Chemistry of Materials 19 (2007) 3850.
[13] P. Su, C. Chao, J.H. Shim, R. Fasching, F.B. Prinz, Nano Letters 8 (2008) 2289.
[14] A.C. Johnson, A. Baclig, D.V. Harburg, B. Lai, S. Ramanathan, Journal of Power Sources 195 (2010) 1149.
[15] X. Chen, N.J. Wu, L. Smith, A. Ignatiev, Applied Physics Letters 84 (2004) 2700.
[16] I. Garbayo, A. Tarancón, J. Santiso, F. Peiró, E. Alarcón-Lladó, A. Cavallaro, I. Gràcia, C. Cané, N. Sabaté, Solid State Ionics 181 (2010) 322.
[17] S. Tekeli, M. Gürü, Ceramics International 34 (2008) 137.
[18] T.S. Zhang, S.H. Chan, W. Wang, K. Hbaieb, L.B. Kong, J. Ma, Solid State Ionics 180 (2009) 82.
[19] M. Aoki, Y.M. Chiang, I. Kosacki, I.J.R. Lee, H. Tuller, Y.P. Liu, Journal of the American Ceramic Society 79 (1996) 1169.
[20] G. Theunissen, A.J.A. Winnubst, A.J. Burggraaf, Journal of Materials Science Letters 8 (1989) 55.
[21] M. de Ridder, R.G. van Welzenis, A.W.D. van der Gon, H.H. Brongersma, S. Wulff, W.F. Chu, W. Weppner, Journal of Applied Physics 92 (2002) 3056.
[22] A. Bernasik, K. Kowalski, A. Sadowski, Journal of Physics and Chemistry of Solids 63 (2002) 233.
[23] G.M. Ingo, Applied Surface Science 70–71 (1993) 235.
[24] K.V. Hansen, K. Norrman, M. Mogensen, Surface and Interface Analysis 38 (2006) 911.
[25] M.F. Yan, R.M. Cannon, H.K. Bowen, Report of Massachusetts Institute of Technology, Report: No. 1, 1976, p. 1.
[26] E.M. Moser, M. Metzger, L.J. Gauckler, Fresenius' Journal of Analytical Chemistry 353 (1995) 684.
[27] M. Gödickemeier, B. Michel, A. Orliukas, P. Bohac, K. Sasaki, L. Gauckler, H. Heinrich, P. Schwander, G. Kostorz, H. Hofmann, O. Frei, Journal of Materials Research 9 (1994) 1228.
[28] A.J. Feighery, J.T.S. Irvine, Solid State Ionics 121 (1999) 209.
[29] S.P.S. Badwal, Solid State Ionics 52 (1992) 23.
[30] G. Petot-Ervas, C. Petot, J.M. Raulot, J. Kusinski, I. Sproule, M. Graham, Ionics 9 (2003) 195.
[31] C.A.H. Chung, K.V. Hansen, M. Mogensen, Ceramic Engineering and Science Proceedings 25 (2004) 407.
[32] A. Hauch, S.H. Jensen, J.B. Bilde-Sorensen, M. Mogensen, Journal of the Electrochemical Society 154 (2007) A619.
[33] K. Norrman, K.V. Hansen, M. Mogensen, Journal of the European Ceramic Society 26 (2006) 967.
[34] K. Vels Jensen, S. Primdahl, I. Chorkendorff, M. Mogensen, Solid State Ionics 144 (2001) 197.
[35] L. Zhang, S.-y. Terauchi, Y. Azuma, T. Fujimoto, Journal of Physics: Conference Series 83 (2007) 012033.
[36] M. Copel, M. Gribelyuk, E. Gusev, Applied Physics Letters 76 (2000) 436.
[37] S.S. Park, et al., Journal of Physics: Condensed Matter 22 (2010) 015002.
[38] P. Peshev, I. Stambolova, S. Vassilev, P. Stefanov, V. Blaskov, K. Starbova, N. Starbov, Materials Science and Engineering B 97 (2003) 106.
[39] S.-C. Hwang, H.-S. Shin, Journal of the American Ceramic Society 82 (1999) 2913.
[40] W. Prusseit, S. Corsépius, M. Zwerger, P. Berberich, H. Kinder, O. Eibl, C. Jaekel, U. Breuer, H. Kurz, Physica C: Superconductivity 201 (1992) 249.
[41] D. Perednis, L.J. Gauckler, Journal of Electroceramics 14 (2005) 103.
[42] O. Wilhelm, S.E. Pratsinis, D. Perednis, L.J. Gauckler, Thin Solid Films 479 (2005) 121.
[43] D. Perednis, O. Wilhelm, S.E. Pratsinis, L.J. Gauckler, Thin Solid Films 474 (2005) 84.
[44] J.L.M. Rupp, B. Scherrer, A. Harvey, L.J. Gauckler, Advanced Functional Materials 19 (2009) 1.
[45] P. Scherrer, Nachrichten von der Königlichen Gesellschaft der Wissenschaft zu Göttingen: Mathematisch–physikalische Klasse 1 (1918) 98.
[46] S.L.D. Lucato, Department of Materials Science, Darmstadt University of Technology, 1998.
[47] F. Mangolini, A. Rossi, N. Spencer, Tribology Letters (2010) 1.
[48] M.P. Seah, W.A. Dench, Surface and Interface Analysis 1 (1979) 2.
[49] M.P. Seah, Surface and Interface Analysis 14 (1989) 488.
[50] J.H. Scofield, Journal of Electron Spectroscopy and Related Phenomena 8 (1976) 129.
[51] R.F. Reilman, A. Msezane, S.T. Manson, Journal of Electron Spectroscopy and Related Phenomena 8 (1976) 389.
[52] K. Berresheim, M. Mattern-Klosson, M. Wilmers, Fresenius' Journal of Analytical Chemistry 341 (1991) 121.
[53] L. Ren You, N.K. Huang, H.L. Zhang, B. Yang, D.Z. Wang, Applied Surface Science 150 (1999) 39.
[54] H. Zhang, N. Huang, Applied Surface Science 133 (1998) 184.
[55] C. Morant, J.M. Sanz, L. Galán, L. Soriano, F. Rueda, Surface Science 218 (1989) 331.
[56] M. Riehl-Chudoba, S. Nishigaki, Y. Huttel, F. Sèmond, P. Brun, P. Soukiassian, Applied Surface Science 65–66 (1993) 840.
[57] F. Giustino, A. Bongiorno, A. Pasquarello, Applied Physics Letters 81 (2002) 4233.
[58] M. Gutowski, J.E. Jaffe, C.-L. Liu, M. Stoker, R.I. Hegde, R.S. Rai, P.J. Tobin, Applied Physics Letters 80 (2002) 1897.
[59] P. Temple-Boyer, C. Rossi, E. Saint-Etienne, E. Scheid, Journal of Vacuum Science & Technology A: Vacuum, Surfaces, and Films 16 (1998) 2003.
[60] S. Habermehl, Journal of Applied Physics 83 (1998) 4672.
[61] A.H. Heuer, V.L.K. Lou, Journal of the American Ceramic Society 73 (1990) 2789.
[62] Y.M. Sun, J. Lozano, H. Ho, H.J. Park, S. Veldman, J.M. White, Applied Surface Science 161 (2000) 115.
[63] J.A. Allemann, B. Michel, H.B. Märki, L.J. Gauckler, E.M. Moser, Journal of the European Ceramic Society 15 (1995) 951.
[64] D.F. Allgeyer, E.H. Pratz, Surface and Interface Analysis 18 (1992) 465.
[65] A.N. Buckley, A.J. Hartmann, R.N. Lamb, A.P.J. Stampfl, J.W. Freeland, I. Coulthard, Surface and Interface Analysis 35 (2003) 922.
[66] A.E. Hughes, N. Janusz, Interfacial phenomena in Y_2O_3–ZrO_2-based ceramics: a surface science perspective, in: Materials Science Monographs, vol. 81, Elsevier, 1995, p. 183.
[67] S. Tekeli, M. Erdogan, B. Aktas, Ceramics International 30 (2004) 2203.